Research Article | Vol. 7, No. 12 | 1 Dec 2016 | BIOMEDICAL OPTICS EXPRESS 4974
Biomedical Optics EXPRESS

Fractional laser photothermolysis using Bessel beams

CHARLES MIGNON, AURA HIGUERA RODRIGUEZ, JONATHAN A. PALERO,* BABU VARGHESE, AND MARTIN JURNA

Department of Personal Care and Wellness, Philips Research, 5656 AE, Eindhoven, The Netherlands
**jonathan.palero@philips.com*

Abstract: Fractional photothermolysis uses lasers to generate a pattern of microscopic columnar thermal lesions within the skin stimulating collagen remodeling. In this paper we investigate the use of Bessel beams as an alternative to conventional Gaussian beams in creating laser photothermal lesions of different aspect ratios in skin. We show for the first time the improved photothermal lesion depth-to-diameter aspect ratio using Bessel beams in *ex vivo* human skin as well as in numerical simulations using electric field Monte Carlo photon transport, finite difference methods and Arrhenius model. Bessel beams allow the creation of deep and narrow thermal lesions necessary for improved efficacy in fractional photothermolysis.

OCIS codes: (140.3300) Laser beam shaping; (140.6810) Thermal effects; (170.0170) Medical optics and biotechnology.

References and links

1. F. Rinaldi, "Laser: a review," Clin. Dermatol. **26**(6), 590–601 (2008).
2. V. V. Tuchin, "Laser light scattering in biomedical diagnostics and therapy," J. Laser Appl. **5**(2), 43–60 (1993).
3. R. R. Anderson and J. A. Parrish, "Selective photothermolysis: precise microsurgery by selective absorption of pulsed radiation," Science **220**(4596), 524–527 (1983).
4. Z. Zhao and P. W. Fairchild, "Dependence of light transmission through human skin on incident beam diameter at different wavelengths," Proc. SPIE **3254**, 354–360 (1998).
5. E. Papadavid and A. Katsambas, "Lasers for facial rejuvenation: a review," Int. J. Dermatol. **42**(6), 480–487 (2003).
6. D. Manstein, G. S. Herron, R. K. Sink, H. Tanner, and R. R. Anderson, "Fractional photothermolysis: a new concept for cutaneous remodeling using microscopic patterns of thermal injury," Lasers Surg. Med. **34**(5), 426–438 (2004).
7. R. G. Geronemus, "Fractional photothermolysis: current and future applications," Lasers Surg. Med. **38**(3), 169–176 (2006).
8. D. J. Goldberg, "New collagen formation after dermal remodeling with an intense pulsed light source," J. Cutan. Laser Ther. **2**(2), 59–61 (2000).
9. Y. Lin, W. Seka, J. H. Eberly, H. Huang, and D. L. Brown, "Experimental investigation of Bessel beam characteristics," Appl. Opt. **31**(15), 2708–2713 (1992).
10. J. Arlt and K. Dholakia, "Generation of high-order Bessel beams by use of an axicon," Opt. Commun. **177**(1-6), 297–301 (2000).
11. G. Indebetouw, "Nondiffracting optical fields: some remarks on their analysis and synthesis," J. Opt. Soc. Am. A **6**(1), 150–152 (1989).
12. A. Elmaklizi, D. Reitzle, A. Brandes, and A. Kienle, "Penetration depth of focused beams in highly scattering media investigated with a numerical solution of Maxwell's equations in two dimensions," J. Biomed. Opt. **20**(6), 065007 (2015).
13. L. Wang, S. L. Jacques, and L. Zheng, "MCML--Monte Carlo modeling of light transport in multi-layered tissues," Comput. Methods Programs Biomed. **47**(2), 131–146 (1995).
14. J. J. Crochet, S. C. Gnyawali, Y. Chen, E. C. Lemley, L. V. Wang, and W. R. Chen, "Temperature distribution in selective laser-tissue interaction," J. Biomed. Opt. **11**(3), 034031 (2006).
15. A. N. Bashkatov, E. A. Genina, and V. V. Tuchin, "Optical properties of skin, subcutaneous, and muscle tissues: a review," J. Innov. Opt. Health Sci. **04**(01), 9–38 (2011).
16. J. A. Pearce, "Relationship between Arrhenius models of thermal damage and the CEM 43 thermal dose," Proc. SPIE **7181**, 718104 (2009).
17. S. A. Sapareto, "The biology of hyperthermia in vitro," in *Physical Aspects of Hyperthermia*, Nussbaum, ed. (1982).

#275410 http://dx.doi.org/10.1364/BOE.7.004974
Journal © 2016 Received 7 Sep 2016; revised 1 Nov 2016; accepted 1 Nov 2016; published 7 Nov 2016

Biomedical Optics EXPRESS

1. Introduction

The photothermal interaction between lasers and biological tissues is the physical basis of tissue ablation, tissue welding and soldering and tissue incision that found their way in a broad range of cosmetic and medical applications [1–3]. The ability to deposit a precise amount of energy in a well-defined region as well as to induce spatially confined thermal lesions in tissues that are highly reproducible render lasers advantage over other tissue heat energy delivery sources. In photothermal laser-tissue interactions the determination of the laser parameters that result in the required depth and diameter of the induced thermal lesion is imperative. It is well known that the penetration depth of the direct heating of tissue depends not only on the laser parameters, such as the laser wavelength, but also on the tissue optical properties which include scattering and absorption coefficients. Moreover for finite-diameter laser beams below a few millimeters, the optical penetration depth in biological tissues turns out to be dependent on the laser beam diameter [4], thus limiting the depth of induced lesions for applications that require generation of microscopic-sized lesions such as in skin fractional photothermolysis [5].

In skin fractional photothermolysis numerous microscopic thermal wounds of controlled diameter and depth are created. These spatially microscopic thermal zones are surrounded by a reservoir of spared epidermal and dermal tissue, allowing for rapid repair of laser-induced thermal injury [6]. Regeneration of new skin cells and tissues commonly known as the skin rejuvenation effect is thus achieved via generation of microscopic thermal zones of the skin layers, including the denaturation of extracellular proteins such as collagen [7,8]. The success of the fractional photothermolysis in rejuvenating the skin relies on creating deep thermal lesions for inducing significant dermal regeneration as well as narrow-diameter thermal lesions to prevent extended epidermal damage minimizing any treatment side effects.

In this paper we present *ex vivo* and numerical results on the use of Bessel beams for creation of high thermal lesion depth-to-diameter aspect ratio. Theoretically Bessel beams are able to penetrate tissues with longer propagation distance and thinner radial extension relative to Gaussian beams [9]. Bessel beams can be created using axicons, phase plates or Fabry-Perot interferometers [10, 11]. Due to their unique properties, these beams offer new fundamental insights in light-tissue photothermal interaction and their use can represent a scientifically interesting and technologically relevant alternative to conventional Gaussian beams. Thus Bessel beams may offer advantages and additional possibilities in creating microscopic thermal zones for skin rejuvenation applications where deep and narrow-diameter profiles are required [7, 12].

We model numerically the photothermal interaction between Bessel beams and skin tissues with particular focus on determining the thermal lesion depth-to-diameter aspect ratio. Bessel beam light transport through skin is modelled though electric field Monte Carlo simulations [13] since the coherence properties of the propagating Bessel beam photons play a big role. The tissue temperature map is obtained using the Finite Difference Method or FDM [14] and the thermal lesion profile is derived using the Arrhenius model. To the best of our knowledge, this paper presents for the first time the use of electric field Monte Carlo simulation to describe photothermal interaction between Bessel beams and biological tissues and to determine Bessel beam-induced lesion size.

2. Materials and methods

2.1 Experimental setup for ex vivo human skin photothermolysis studies

To demonstrate the advantage of using Bessel beams over conventional Gaussian beams for skin fractional photothermolysis, we built an experimental setup comprising a 1550 mW laser diode operating at 1435 nm and an optical beam shaping system to produce ~1 mm input beam diameter for delivering Bessel or Gaussian beam on to an *ex vivo* human skin sample. We controlled the applied laser energy by controlling the pulse duration of the laser. In the

Biomedical Optics EXPRESS

experiments, we used 11 mJ, 16 mJ, 31 mJ, 47 mJ, and 62 mJ by setting the pulse durations to 7 ms, 10 ms, 20 ms, 30 ms and 40 ms, respectively. To enable comparison between thermal lesions created by Bessel and Gaussian beams, we configured the optical beam shaping system to produce equivalent beam waist at full-width-at-half maximum (FWHM) of ~5 μm on the surface of the human skin sample. The Bessel beam was generated using an axicon with an angle, α = 5° producing an extended beam with a theoretical propagation distance in air of ~16 mm and the Gaussian beam using a lens with a long focal length of 11 mm producing a beam with a Rayleigh range in air of ~50 μm. The beams were focused onto the skin such that the peak axial intensity is at the surface of the skin.

2.2 Sample preparation

Freshly excised human abdominal skin tissue samples were obtained with consent from the donors. Prior to the actual treatment, two *ex vivo* samples of ~5 mm × ~10 mm with thickness of ~1 mm were prepared, one sample for each laser beam geometry. For each sample, eleven lesions were created for each of the five different laser energy settings. The tissues were cryosectioned and cellular damage was evaluated in frozen sections using nitro-blue tetrazolium chloride (NBTC), a lactate dehydrogenase (LDH) activity stain. The analysis of the histological lesions was performed using a microscope (10 × objective, Leica DM IL LED).

2.3 Photon transport simulations via phase Monte Carlo

Monte Carlo simulations were performed using a three-layer 3D-skin model (see Fig. 1(A)) to obtain the photon absorption density map. The medium is assumed to be infinite in the plane perpendicular to the propagation axis. We used the Henvey-Greenstein distribution for the scattering phase function and the optical properties of the skin model layers are summarized in Table 1 [15]. In addition to a classic Monte Carlo model as described in reference [13], the electric field phase of each photon packet was registered allowing Bessel beam coherence properties, i.e. optical interference pattern to be modeled. In all simulations, 10^7 photons are injected into the sample at a grid resolution of 1 μm. In order to reach a sufficient resolution for the creation of Bessel beams in the skin, we averaged several absorption maps from 10 simulations performed with 10^7 photon packets.

For each step in the simulation, the light intensity for each grid element u is described by:

$$Intensity_u = \left| \sum_{j \in u} W_j \cos\left(\phi_j\right) + i\left(\sum_{j \in u} W_j \sin\left(\phi_j\right) \right) \right|^2$$

where ϕ is the phase of the photon packet, W_j is the current weight of photons. To generate the Bessel beam profile in the skin, a photon packet j is randomly sampled from the skin surface carrying the associated photon phase described by:

$$\phi_{0,j} = \frac{2\pi n_{axicon}}{\lambda}(R_{axicon} - R_j)tan\alpha_{axicon}$$

where n_{axicon}, R_{axicon} and α_{axicon} are the refractive index, radius and inner angle of the axicon, respectively, and R_j is radial distance of the photon j from the optical axis. In the simulations, we used a wavelength of 1435 nm, a beam diameter of 1 mm and an axicon with an angle α = 5°.

Table 1. Optical properties of skin model layers at 1435 nm [15].

Layer	μ_a (cm^{-1})	$\mu_s'(cm^{-1})$	g	n	Thickness (μm)
Stratum corneum	3.17	22.20	0.91	1.5	10
Viable epidermis	26.4	22.20	0.91	1.42	50
Dermis	25.6	13.55	0.91	1.36	2940

Biomedical Optics EXPRESS

2.4 Lesion size determination

The time-resolved tissue thermal maps (Fig. 1(C)) is obtained from the photon absorption map, as shown in Fig. 1(B), by solving the bio-heat equation based on Finite Difference Method. FDM discretization of the heat equation consists of two steps, one is temporal discretization and the other one is the approximation of the spatial Laplacian. In this model, we used the four-pixel nearest neighbor definition of approximated Laplacian [14]. Temporal discretization is based on a linear relation assumption between the value in one time step of the temperature T_{n+1} for each pixel with the previous temperature T_n. The values of the skin thermal constants used are shown in Table 2. The photon absorption map is median-filtered prior to FDM to a spatial resolution of 10 µm resulting in a time increment of 10 µs.

Table 2. Skin thermal constants used in the numerical simulation

Thermal model parameters	Values
Thermal Conductivity k ($W \cdot m^{-1} \cdot K^{-1}$)	0.25
Density ρ ($kg \cdot m^{-3}$)	1200
Heat capacity c ($J \cdot g^{-1} \cdot K^{-1}$)	3.6
Convection constant ($W \cdot m^{-1} \cdot K^{-1}$)	4.33

The described implementation of temporal and spatial approximations in applying the bio-heat equation can be formally formulated with the Crank-Nicolson linear algebra method allowing each increment to be computed at relatively short times. The resulting time-resolved tissue thermal map (Fig. 1(C)) allows observation of the temperature during direct heating of the tissue with the laser as well as the indirect heating of unexposed tissue regions by thermal diffusion.

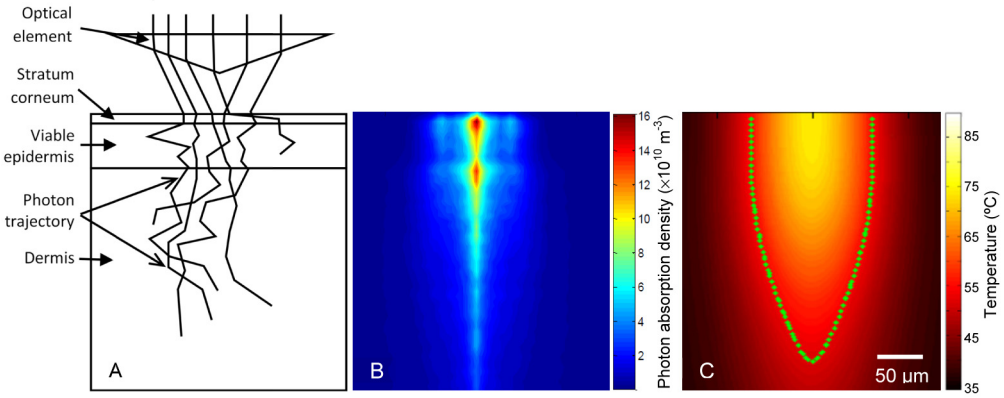

Fig. 1. A: Schematic diagram of a cross-section of the three-dimensional model used in the Monte Carlo simulations comprising a three-layer skin model and an optical element. B: A typical numerical photon absorption map. C: A typical skin thermal map in pseudocolor (see Visualization 1). The iso-damage (10%) contour is also shown as dotted green line. Scale bar is 50 µm for all images.

Based on the time-resolved thermal map the damage zone within the tissue was defined using the Arrhenius model [16]. The global description of Arrhenius model and the general rate equation were used to estimate the damage integral. This integral is evaluated from the evolution of spatiotemporal temperature distribution, taking into account a breakpoint at 43°C of the Arrhenius pre-exponential factor, A, the activation energy E_A and the critical temperature T_{crit} [16,17]. They were respectively set to 1.67×10^{280} s^{-1}, 1.71×10^{6} $J \cdot mol^{-1}$ and 45.6 °C for tissue temperature under the breakpoint and 2.84×10^{99} s^{-1}, 6.19×10^{5} $J \cdot mol^{-1}$ and 51.4 °C for tissue temperature over the breakpoint. The damage probability P(%) which is defined as the exponential of the damage integral, was used to demarcate the thermally damaged zones leading to the lesion dimension. Pearce et al. [16] describes the

Biomedical Optics EXPRESS

difficulty to choose a damage threshold for evaluating the thermal damage in tissue and suggest that 10% damage could already be an useful marker of irreversible thermal alteration. Here we set the damage probability threshold to be 10% [16] which is visualized in the thermal maps as iso-damage contour lines (Fig. 1(C), dotted green line) . This damage threshold was validated by direct comparison of simulated and experimental data.

3. Results and discussion

Shown in Fig. 2(A) to 2(D), are NBTC-stained histological sections depicting typical photothermal lesions created in *ex vivo* skin using a Bessel beam at different energies, 11 mJ, 16 mJ, 31 mJ and 47 mJ, respectively. The photothermal lesions (region bounded by red dotted lines, Fig. 2) are visually identified as regions with loss in blue stain due to loss in tissue viability. We observe that the lesion depth is larger than the lesion diameter for all laser energies and that the lesion diameter and depth increase with increasing laser energy of the Bessel beam. Moreover, the lesions are generated by Gaussian beams are generally wider than the Bessel-beam-generated lesions using equivalent energies (see Fig. 3). These observations are more evident in Fig. 4 (filled symbols) in good agreement with the results of the simulations (hollow symbols). It is also evident that the increase in depth with increasing laser energy is slightly steeper than the increase in lesion diameter for energies <20 mJ, while increase in both parameters gradually level off at higher energies. Since in the experiments the energy is varied by varying the pulse duration at fixed laser powers, the saturating behavior at higher energies may in fact be an effect of skin thermal relaxation response. Due to thermal diffusion during a light pulse, the local temperature rise due to direct absorption of light is modulated by thermal diffusion to the surrounding tissue resulting in a steady-state temperature response at times longer than the thermal relaxation time. This in effect results in a steady-state thermal profile consequently limiting the lesion growth dimension, both depth and diameter at long pulse durations. Based on the fitted curve shown in Fig. 4(A) (red line: depth, blue line: diameter) using the form: $\mathrm{D} = \mathrm{D}_0 + \mathrm{A}\left(1 - \mathrm{e}^{-E/k}\right)$, we derive the relevant exponential curve constants as $k_z^{Bessel} = 35\,mJ$ and $k_r^{Bessel} = 23\,mJ$, for the Bessel-generated lesion depth and diameter, respectively. Converting these energy values to pulse duration values lead to the Bessel-generated lesion growth time constants, $\tau_z^{Bessel} = 22\,ms$ and $\tau_r^{Bessel} = 15\,ms$, for the depth and diameter, respectively.

The depth-to-diameter aspect ratio based on histological measurements are found to be in good agreement with the calculated depth-to-diameter aspect ratio and that the numerical result measurements show exponentially decrease for energies >20 mJ. This suggests that the advantage of using Bessel beams to produce high depth-to-diameter aspect ratio is optimal at low laser energies or short pulse durations, while at high energies or long pulse durations, the aspect ratio becomes independent of the laser energy. Based on the best fit exponential decay curve (Fig. 4(B), line) within the experimental range of laser energies used, the depth-to-diameter aspect ratio is calculated to be approach a value of 1.17 for high energies.

Biomedical Optics EXPRESS

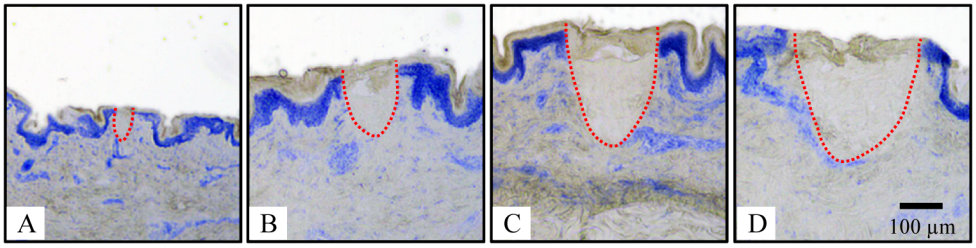

Fig. 2. NBTC-stained histological sections of *ex vivo* skin showing typical photothermal lesions (region bounded by red dotted lines) created using a Bessel beam at 11-, 16-, 31- and 47-mJ, from A to D, respectively. Scale bar is 100 µm for all images.

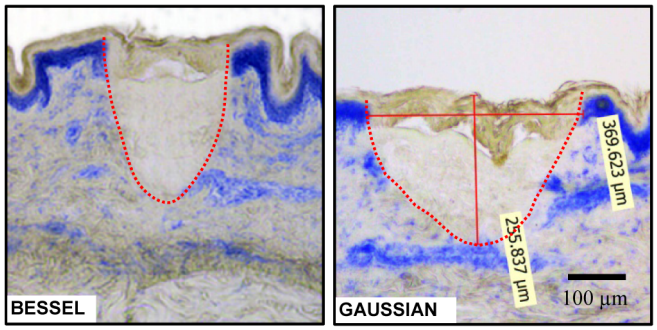

Fig. 3. NBTC-stained histological sections of *ex vivo* skin showing photothermal lesions (region bounded by red dotted lines) created using a Bessel beam (left) and a Gaussian beam (right) with equivalent incident beam waist, pulse energy at 31 mJ and pulse duration of 20 ms. Scale bar is 100 µm for both images.

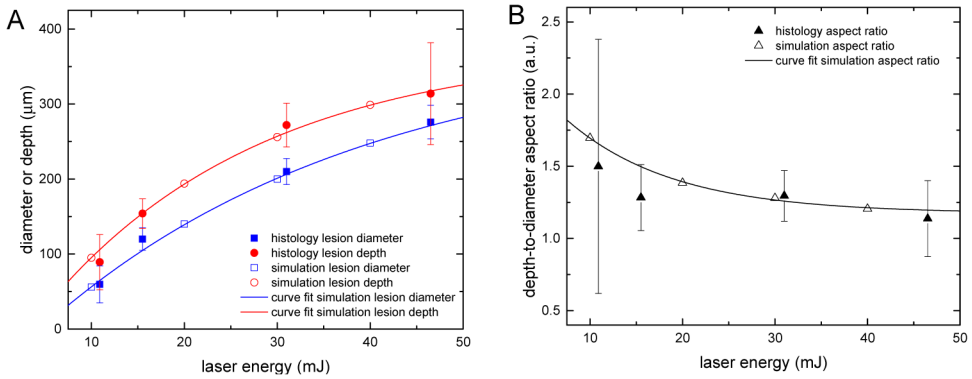

Fig. 4. A: Average Bessel-generated lesion diameter (blue filled squares) and depth (red filled circles) for different laser energies measured from skin histological sections. Shown also lesion diameter (blue hollow squares) and depth (red hollow circles) derived from numerical simulation results, and the curve fit lines. B: Calculated depth-to-diameter aspect ratio from histological measurements (filled triangles) and numerical result measurements (hollow triangles) as a function of laser energy.

In contrast to the lesions generated by Bessel beams, the lesion depth is less than the diameter for the Gaussian beam-generated *ex vivo* lesions as shown in Fig. 4(A). To exemplify the difference, using the same laser energy of 31 mJ (see typical lesions in Fig. 3), while the depth of lesions generated by Bessel and Gaussian beams are on the same order of magnitude, i.e. 272 ± 29 µm (mean ± SD) and 261 ± 54 µm, respectively, the Bessel beam generated narrower lesions (210 ± 17 µm) than the Gaussian beam lesion (381 ± 30 µm). We note here that at laser energies <31 mJ, no discernable lesions were observed in the skin

Biomedical Optics EXPRESS

histological sections. Based on the fitted curve (Fig. 5(A)), red line: depth, blue line: diameter) to the *ex vivo* lesion measurement data using the same exponential form as in the curve-fitting for the Bessel lesion data, we derive the relevant exponential curve constants as $k_z^{Gaussian} = 24\,mJ$ and $k_r^{Gaussian} = 25\,mJ$, which correspond to Gaussian-generated lesion growth time constants, $\tau_z^{Gaussian} = 16\,ms$ and $\tau_r^{Gaussian} = 16\,ms$, for the depth and diameter, respectively. Here, we observe that the lesion growth time constants for the diameter between the Bessel- and Gaussian-generated lesions are markedly similar, which is in fact not unexpected since the diameters of the two beams are configured to be the same. However, the lesion growth time constants for the depth are significantly different wherein $\tau_z^{Bessel} > \tau_z^{Gaussian}$. We can attribute this difference in depth growth time constants to the difference in optical propagation depths of the two beams, wherein Bessel beams can penetrate deeper in skin than Gaussian beams. Knowing that in general thermal relaxation time in the *z*-direction is proportional to the penetration depth squared, we hypothesize that the optical penetration depth determines the thermal lesion growth behavior.

The computed depth-to-diameter aspect ratio for the Gaussian beam-generated lesions are found to be significantly lower than the aspect ratio for the Bessel beam-generated lesions. At 31 mJ, Bessel beam-generated lesion aspect ratio (1.3 ± 0.18) is ~2-fold more favorable than the Gaussian beam-generated lesion aspect ratio (0.69 ± 0.15).

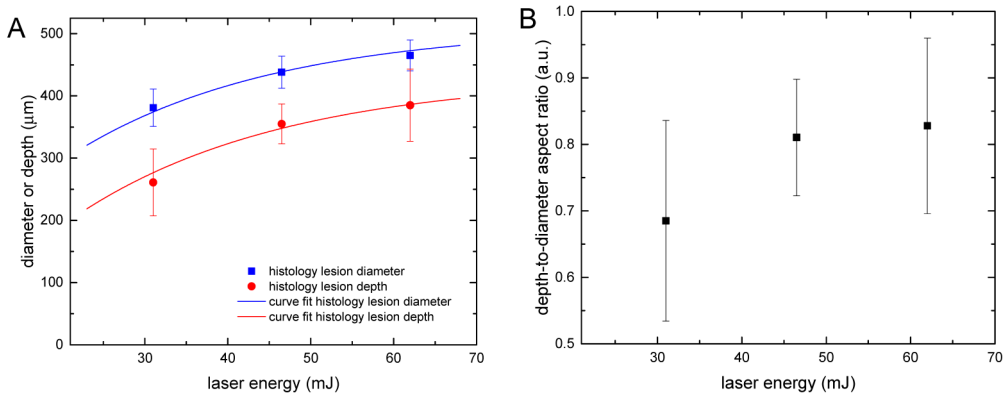

Fig. 5. A: Average Gaussian beam-generated lesion diameter (blue filled squares) and depth (red filled circles) for different laser energies measured from skin histological sections. The best curve fit is also shown (solid lines). B: Calculated depth-to-diameter aspect ratio from histological measurements (squares) as a function of laser energy.

The experimental results of the study clearly shows the advantage of Bessel beams over Gaussian beams in terms of generating laser-induced photothermal lesions with higher depth-to-diameter aspect ratios. These results also provide evidence that Bessel beams are able to penetrate tissues with longer propagation distance and thinner radial extension relative to Gaussian beams [9].

The ability of Bessel beams to penetrate tissues, which are highly scattering, at relatively long distances is due to its capability to self-reconstruct or self-heal along the axial direction of propagation. Due to its plane-wave focus geometry, scattering and absorbing obstacles along the beam path have minimal impact to the Bessel beam axial profile. In Gaussian beams however, such obstacles along the beam path dramatically distort the beam axial profile.

4. Conclusion

In this paper we have demonstrated the advantage of using Bessel beams in generating skin photothermal lesions with higher depth-to-diameter aspect ratio relative to Gaussian beam-generated lesions. The experimental results of human skin ex vivo fractional

Biomedical Optics EXPRESS

photothermolysis are found to be in agreement with the results of numerical modeling based on electric field Monte Carlo for fractional photothermolysis. To the best of our knowledge this paper presented for the first time the use of electric field Monte Carlo simulation to describe photothermal interaction between Bessel beams and biological tissues and to determine Bessel beam-induced lesion size. The results of this study provide an opportunity to improve the efficacy of fractional photothermolysis for skin rejuvenation where creation of microscopic thermal zones with deep and narrow-diameter profiles are more favorable.